

We are IntechOpen, the world's leading publisher of Open Access books Built by scientists, for scientists

6,900

Open access books available

185,000

International authors and editors

200M

Downloads

Our authors are among the

154

Countries delivered to

TOP 1%

most cited scientists

12.2%

Contributors from top 500 universities



WEB OF SCIENCE™

Selection of our books indexed in the Book Citation Index
in Web of Science™ Core Collection (BKCI)

Interested in publishing with us?
Contact book.department@intechopen.com

Numbers displayed above are based on latest data collected.
For more information visit www.intechopen.com



Comparison of Aerodynamic Effects Promoted by Mechanical and Fluidic Miniflaps on an Airfoil NACA 4412

M. Casper¹, P. Scholz¹, J. Colman²,
J. Marañón Di Leo², S. Delnero² and M. Camocardi²

¹*Institute of Fluid Mechanics, Braunschweig Technical University*

²*Boundary Layer and Environmental Fluid Dynamics Laboratory,
Engineering Faculty, National University of La Plata*

¹*Germany*

²*Argentina*

1. Introduction

Miniflaps, often called “Gurney flaps” have been introduced by the US race-car driver Dan Gurney, who used these small-scale (typically 1% of chord), highly deployed flaps at the trailing edge of the rear spoiler of his racing car. He experienced a significant increase of lift.

Since then Gurney flap were studied by many authors [2]- [5], all confirming an increase of the lift and lift-to-drag ratio and a reduced form drag obtained at high lift coefficients compared with the same airfoil without the flap. Giguère et al [6], described experimentally the aerodynamic behavior of these flaps scaling their height with the boundary layer thickness.

Although Gurneys are extensively used in race-car aerodynamics, application on aircraft is rather uncommon. That might be attributed to the fact that it is very intricate to design deployable flaps in the very thin trailing edge region of common airfoils and the effectiveness of Gurney flaps does not justify the effort or additional weight, respectively. Therefore it is of great interest to explore fundamental methods to increase the effectiveness.

The wake immediately downstream a common lifting airfoil is asymmetric due to the different external and boundary layer flows on the pressure and suction surfaces of the airfoil. The structure in this near wake region is influenced by aero dynamical loading and airfoil characteristics.

Downstream of the trailing edge of a normal lifting airfoil the downwash diminishes rapidly. Hah and Lakshminarayana, in their experimental and numerical study about the near wake of a lifting airfoil [1], confirmed that the asymmetric wake becomes nearly symmetric after only one chord length downstream of the trailing edge. These authors reported also that the far wake shows a roughly symmetric wake structure in which the airfoil features and aerodynamic loads does not influence the wake development anymore.

Also, the fundamental understanding of the lift increase generated by Gurney-type miniflaps is connected to a wake phenomenon: A counter-rotating vortex pair will develop behind the blunt trailing-edge generated by the Gurney flap. These vortices induce streamlines resembling a smooth, “virtual” aerodynamic prolongation of the airfoil, allowing to retain a pressure difference at the trailing edge and thus adding a virtual camber by shifting downward the rear stagnation point where the Kutta condition must be applied. A more detailed description of the flow structures in the Gurney flap flow-pattern obtained by experiments with laser Doppler anemometry (LDA) was reported [7], [8]. Aspects of the behaviour of airfoils equipped with miniflaps with different lengths were described in [9], reported about the influence of free stream turbulence structure on these devices.

However, the unsteady nature of the counter-rotating vortices behind the miniflap complicates this “time-averaged” point of thinking. It is known that the highly unsteady nature of flows associated with vortex shedding make theoretical understanding difficult. It should be mentioned that up to date there are no theories for predicting the drag coefficient as a function of Reynolds number in vortex shedding conditions of extremely basic bodies such as circular cylinders.

In some studies about aerodynamic efficiency of Gurney flaps it is common to find the assumption that the effect of the asymmetry of the vortices on lift to drag ratio is detrimental. In order to attain a drag reduction by “*stabilizing the wake*” some authors suggest the use of span-wise holes, slits, serrated flaps and wake-bodies [10], [11], while other recommend to eliminate straightforward the double row of counter-rotating vortices of the wake behind a Gurney type miniflap [12].

2. Our proposal

We hypothesize that different perturbations introduced near the separating regions of the shear layers from the pressure and suction sides of an airfoil introduce asymmetry in the vortex structures of the near wake region able to produce lift enhancing effects.

The turbulent flow behind the blunt trailing edge of an airfoil with a Gurney flap, involves turbulent boundary layers separating at the airfoil edges, developing into shear layers which rollup into discrete vortices. The negative and positive vorticity from the separating boundary layers is packed into the rolling up shear layers developing into vortices that merge downstream at the vortex shedding frequency. The Kutta condition is obviously not fulfilled at the blunt trailing edge, but at a moving stagnation point that appears rearward and downward from the trailing edge of the airfoil. Each time a vortex is shed into the wake circulation is produced. According Kelvin’s theorem, the periodic vortex shedding from the trailing edge into the wake is connected to time variations of the strength of the bound vortex, which in turn deviate the velocity field, inducing periodic variations of the angle of attack of the incident velocity. Let us concentrate on the near wake flow behind blunt bodies. A periodic shedding of equal counter rotating vortices creates a periodic up and downward lift and periodic drag variations. A body with a Karman type vortex wake, experiences a periodic fluctuating upward and downward lift coupled to the regular counter rotating vortex shedding which induces upward and downward deflections of the flow. Hence, a symmetric Karman type vortex street pattern alone could not contribute to a steady lift.

The lift required in common aeronautic applications involves a preferential deviation of the oncoming flow visualized by the known up and downwash before and behind a wing. If we focus on the downwash of the flow behind the trailing edge of a conventional lifting airfoil, we appreciate that more lift is connected with more downwash. Therefore, a vortex street in itself is not detrimental, but asymmetry of the wake is crucial. E.g. in the near wake region the initial eddies of the vortex street rotating in one direction, should be much stronger than the initial eddies rotating in the opposite direction such that a preferential deflection of the wake connected to a time averaged steady lift will occur.

Therefore it is worthwhile to explore the vertical motion and dynamics in the near-wake of an airfoil with a Gurney-type miniflap. It is even more worthwhile to introduce a mechanism that will be able to actively influence and maximize the asymmetry of the wake in order to increase the additional lift gained by the miniflap. Such mechanism can be either a mechanically moving Gurney or a fluidic device that can be switched off and on by the means of valves.

3. Experimental procedure

In the following works, the experiments with the wing model, equipped inside with a electromechanical system which bring oscillating up-down movement to a miniflap, were carried out at the Boundary Layer and Environmental Fluid Dynamics Laboratory (LaCLyFA) closed circuit wind tunnel, at the Faculty of Engineering, National University of La Plata, Argentina. In each work there will be indicated the specific Reynolds number but, in all cases, corresponds to *low Reynolds number aerodynamics*. At LaCLyFA, instantaneous velocities at the near wake were measured by a six channel Dantec Streamline hot-wire constant temperature anemometer (X-wire type probes).

Complementary to these tests with a mechanical gurney experiments, another ones using a fluidic gurney are conducted in the low speed facility at the Institute of Fluid Mechanics (ISM) at Braunschweig Technical University. The model tested, with the NACA 4412 airfoil, has a chord of 240mm. Seven fast switching valves are integrated into the model, the air is guided from the vales through individual "diffusers" into a small settling chamber and then through a small, wall-normal slit into the flow. The position of the slit is $x/c=0,92$, that is 8% upstream of the trailing edge. Thus, the position of this fluidic gurney is similar to the mechanical gurney at the LaCLyFA. The air emitted through the slit acts just like a jet-flap or a Gurney flap, respectively. Through the valves the effect can be switched on and off, where the valves are small electro-magnetic devices (FESTO MHJ), that are able to produce rather high frequencies of up to 1 kHz in a very reproducible manner. The airfoil is equipped with 30 pressure taps to measure the pressure distribution.

4. Experimental results

4.1 Fluidic mini-flap

Tests with a fluidic Gurney are conducted in the low speed facility at the Institut für Strömungsmechanik (ISM) at Technische Universität in Braunschweig, Germany. The facility is an atmospheric open-jet return-tunnel with a jet diameter of 0.5 m. The jet collector is located 0.98 m downstream of the nozzle. The tunnel has a frequency controlled drive system with 22 kW, enabling a maximum velocity of 60m/s. For the measurements herein

however, velocities of 26 m/s and 39 m/s were used to establish Reynolds-identity with the data taken at LaCLyFA. The tunnel velocity is controlled by the differential pressure over the nozzle.

The airfoil is mounted with endplates in the center of the wind tunnel jet. The airfoil model has a chord of $c=230$ mm, it is equipped with 30 static pressure taps near the center section. To create the fluidic gurney-jet six solenoid fast-switching valves are integrated into the airfoil: the air is guided from the vales through individual “diffusers” into a small settling chamber and then through a small, wall-normal slit into the flow. The position of the slit is $x/c = 0.92$, that is 8% upstream of the trailing edge. Thus, the position of this fluidic gurney is identical to the mechanical gurney at the LaCLyFA. The slit itself is manufactured using a laser cutting technique into an “insert-sheet” made of stainless steel. The slit size is 0.2mm, because of the manufactured technique the slit size can be controlled very accurately. Through the valves the effect can be switched on and off, where the valves are small electromagnetic devices (FESTO MHJ) that are able to produce rather high frequencies of up to 1 kHz in a very reproducible manner. The valves are controlled by a square signal with the desired frequency synthesized by a standard frequency generator.

Figure 1a shows a sketch drawing highlighting the fluidic gurney-system. The airfoil body is manufactured using a 3D-printing technique (“Stereo lithography”), where all air ducts, pressure taps and settling chambers are printed in one step. To get access to the valves located inside the airfoil, the body features two large hatches on the pressure side that can be closed with covers representing the airfoil geometry (see also Figure 1b).

The static pressure distribution was measured by means of a custom build multi-channel pressure scanner, based on sensors with a total pressure range of ± 250 mbar. Lift can be determined by integration of the static pressure distribution.

The data was corrected for open-jet effects following the procedure described in [13]. The relevant factors are $G_0=1.0$, $G_1=0.33$ for the streamline-curvature correction and $\varepsilon_S=-0.00867$ for solid blockage. Following that procedure the angle of attack that will be compared below (specifically 5°) represents the same aerodynamic condition, although the geometrical angle of attack of the airfoil in the wind tunnel stream is 10° .

Flow analysis was conducted using a PIV setup, consisting of a Litron Nano-T 200mJ/Puls double-pulse Laser and a LaVision Imager Pro X 11M camera with 11 Mega-Pixels. The PIV data has been acquired, correlated and analyzed using the “DaVis 7” software package from LaVision. Correlation was done with an iterative multi-grid procedure with initial window size of 128 Pxs² and final size of 64 Pxs², both with 50% window overlap. Final resolution of the vector field is 2.2 mm. In the case of a pulsing Gurney jet the acquisition trigger of the PIV-system was controlled by the frequency generator of the valves, enabling phase-locked measurements. Due to the sidewall-plates surrounding the airfoil optical access is limited to the region shown in the figures below.

Data has been acquired for a reference case (no fluidic Gurney jet), a statically blowing Gurney jet (comparable to a “classical” mechanical Gurney that is deployed stationary) and a pulsing Gurney jet. Pulsing frequency is F1 ($f^+=1.32$). For the pulsing jet three different phase positions were measured, namely $\lambda=0.13 \cdot T$ (or 45°), $\lambda=0.49 \cdot T$ (or 180°) and $\lambda=0.77 \cdot T$ (or 275°), where T is the periodicity time of the pulsing.

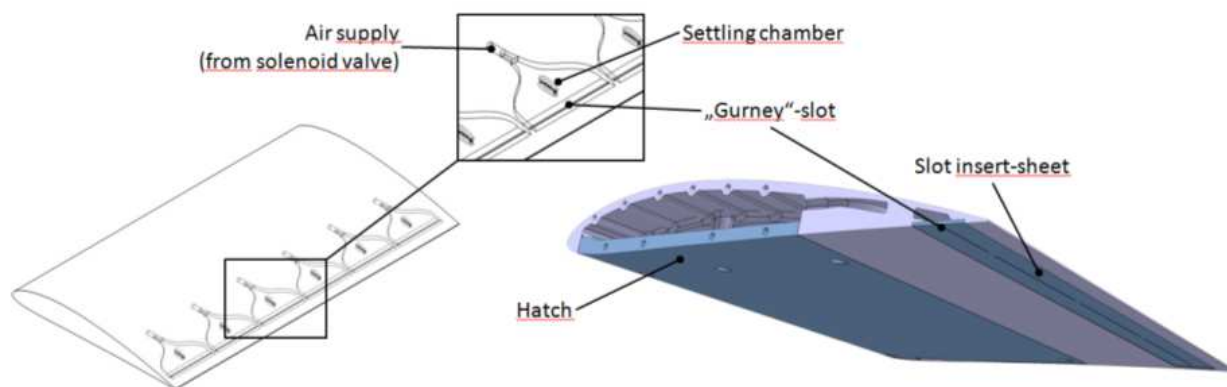


Fig. 1a. Sketch of the fluidic-gurney airfoil showing the air supply system

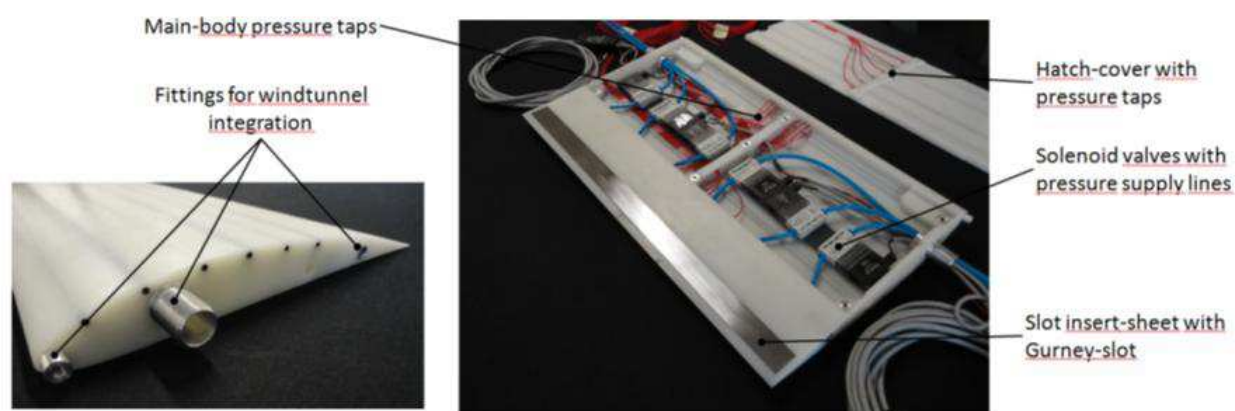


Fig. 1b. Photographs of the airfoil model with fluidic mini-flap system

Results (medium to far wake region)

The following figures highlight the vorticity field that was computed from the velocities. The vorticity field was averaged over 500 individual measurements for each of the cases. Vorticity is in an arbitrary unit (based on the image scaling), which is consistent over all measurements.

Figure 2 to 5 highlights the transversal vorticity, normalized by the peak vorticity measured for the dynamic gurney jet, in comparison for the reference case (without Gurney jet), the statically blowing Gurney jet and the pulsed Gurney. The pulsing frequency is again F1 (reduced frequency $f^+=1.3$). The time averaged flow rate for the pulsed Gurney and the static Gurney is the same. Solid lines and/or open symbols represent positive vorticity, dashed lines and/or filled symbols represent negative vorticity. Note that for the two cases reference and static Gurney the vorticity over x/c is essentially a continuous curve, since the data is averaged over time. For the pulsed Gurney the data points represent the peak vorticity (and respective position) of individual vortices that have rolled up in the shear layer. These vortices have been manually isolated piece by piece, noting vorticity and position. This analysis has been done with different phase angles (see Figure 6), thus the data represents the averaged peak vorticity of local vortices. Furthermore it must be noted that positive vorticity is “rotation counterclockwise”, thus positive vorticity should be connected to a lift increase at the airfoil, while negative (rotation clockwise) vorticity to lift decrease.

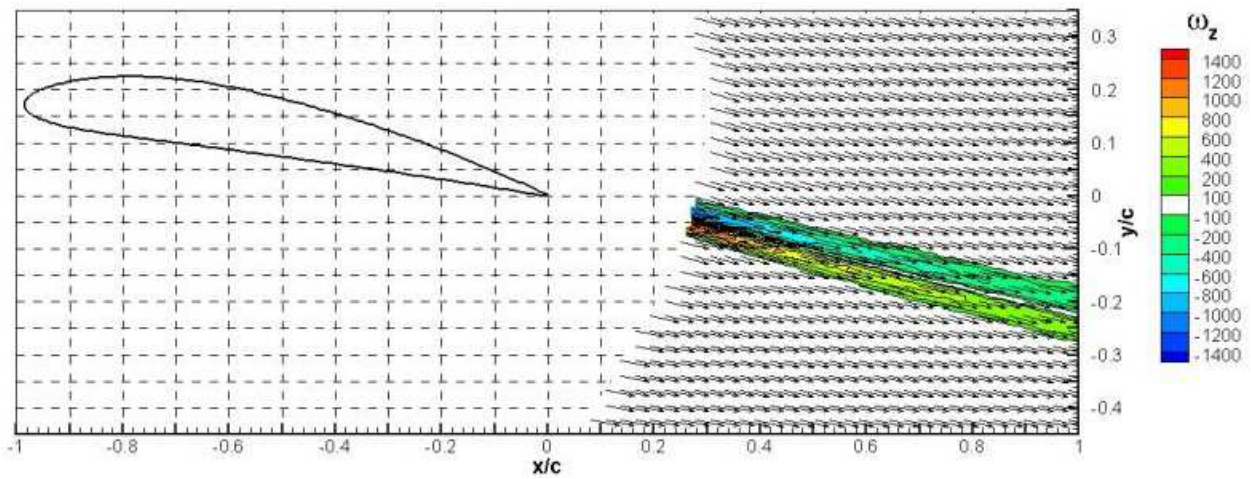


Fig. 2. Vector-field and transversal vorticity (every 3rd vector displayed) for the reference case (no Gurney)

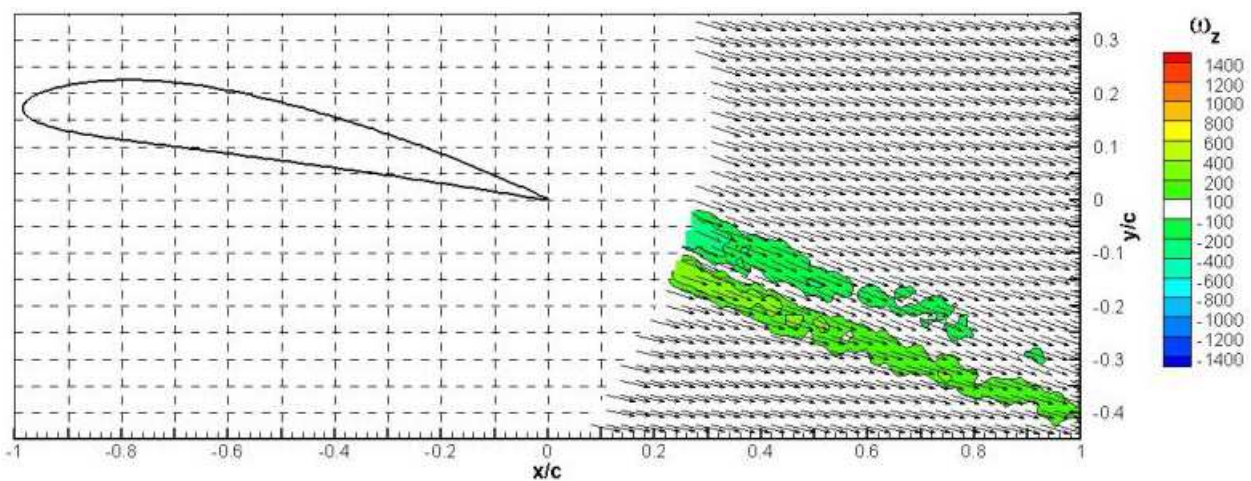


Fig. 3. Same as above for the statically blowing fluidic Gurney jet

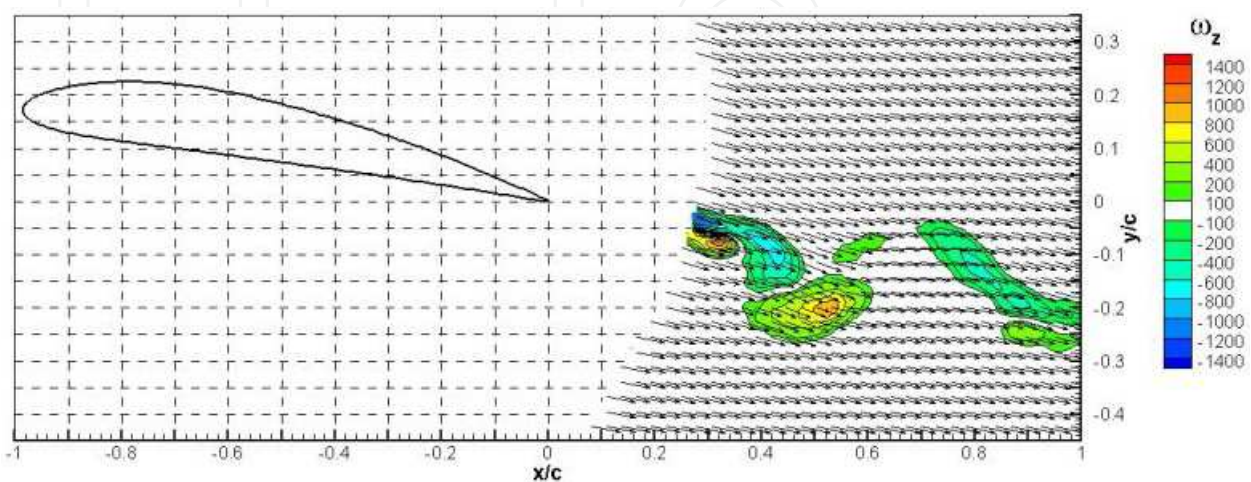


Fig. 4. Same as above for the pulsed fluidic Gurney jet, pulsing $f^+=1.32$

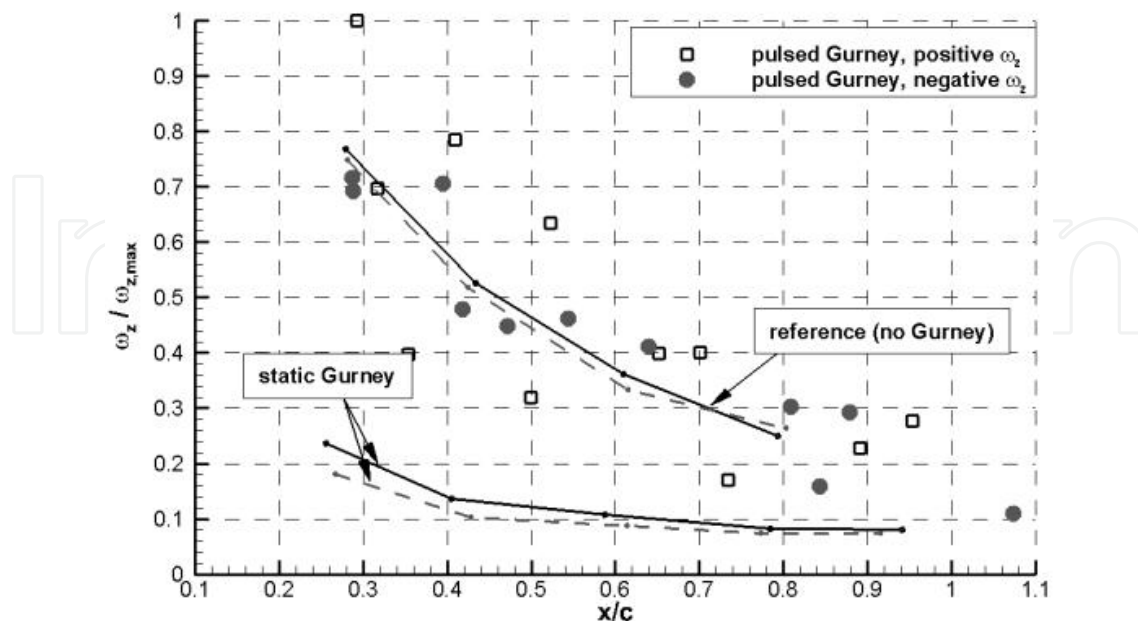


Fig. 5. Transversal vorticity over downstream distance for the different cases

Some different conclusions can be drawn from the plot: For the reference case the wake is almost symmetric, with however, consistently slightly weaker negative vorticity. The same is true for the statically blowing Gurney jet, where the total level of vorticity is significant lower, but the asymmetry is slightly more pronounced compared to the reference case.

The individual vortices emanating from the pulsed Gurney jet are quite strong compared to the two other cases. Although it is evident that with only three phase angles it is not possible to draw a continuous line for the peak vorticity of the vortices carried out downstream, most of the vortices rotating counterclockwise (positive) are stronger than their negative counterparts. This is especially true the smaller x/c is (e.g. the closer we get to the near wake region), while respectively with increasing x/c also the difference in positive and negative vorticity vanishes and the vortices become more and more symmetric.

Following the above stated hypothesis this is due to the lift that the airfoil creates. For all cases the wake asymmetry vanishes somewhat around $x/c=1$, that is one chord length downstream of the airfoil.

The Figure 6 highlights the temporal evolution of the vorticity in a spatially resolved, closeup view of the wake. It is clearly visible at time $0.13 \cdot T$ that a almost isolated, rather strong vortex develops at the trailing edge, when the Gurney jet is turned on. This vortex rotates counterclockwise and thus contributes to lift or is connected to a positive lift increase at the airfoil, respectively. This vortex trails downstream and decays slowly. In the later stages a quasi-static wake develops, which is quite similar to the wake without Gurney, since this is connected to the part of the period where the Gurney jet is switched off. Note also that the most pronounced peak negative vorticity occurs more in this quasi-static part of the period, whereas the peak positive vorticity is connected to the “puff” that comes from the suddenly starting Gurney.

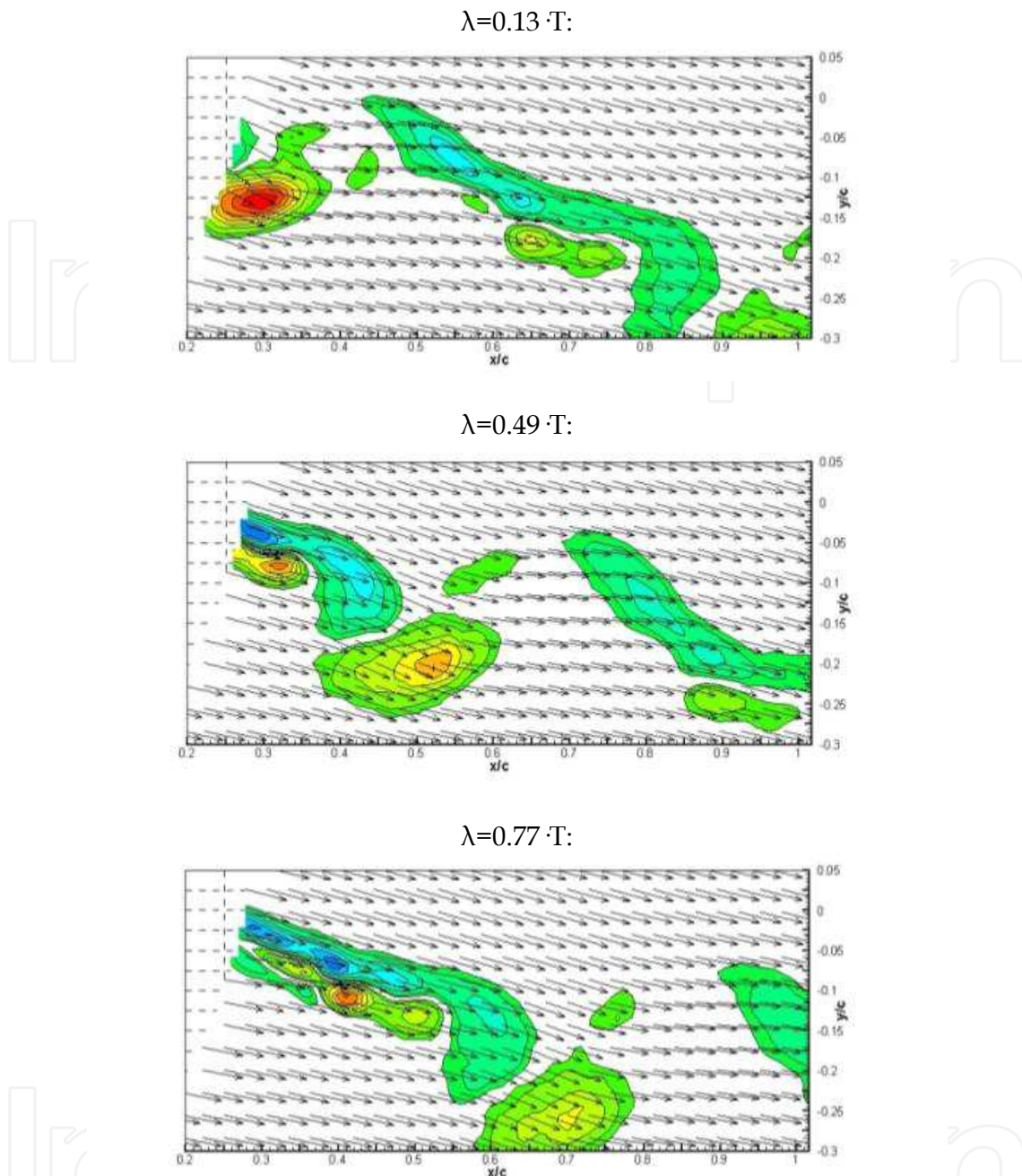


Fig. 6. Evolution of vorticity in time (phase locked), pulsed Gurney jet $f^+=1.3$; vorticity color same as in Figure 2

4.2 Mechanical mini-flap

The untwisted wing model tested, of 60cm chord (c) and 80cm wingspan had a NACA 4412 airfoil. The Reynolds number, based upon the wing chord and the mean free stream velocity were 326.000 and 489000, based upon the mean free stream velocity (at 1.5m ahead the model at its height) and the model chord, corresponding to values of it of 10m/s and 15m/s respectively, depending on the test. The turbulence intensity was 1.8% (minimum turbulence intensity of the wind tunnel). The closest possible distance from the trailing edge, for the Gurney flap position, was determined by the implemented mechanism inside the model.

The model has a mini-flap Gurney type located on the lower surface near the trailing edge, used as passive and active flow control device. As an active device an up-down movement was designed, geared by an electromechanical system. Such mechanism employed a continuous current small electric motor with a crankshaft fixed at its axle, provided with a high capacity rotation velocity sealed bearing. The bearing, when the motor rotate, impinge an up-down movement to the mini-flap (composite plate) placed along wingspan at 8%*c* from the trailing edge. Mini-flap height was 1.3%*c*. Thus, the mini-flap was capable to make an oscillatory up-down movement from the lower surface (0mm displacement) to the maximum amplitude (10mm). The electric motor had a constant voltage variable frequency power supply, in order to be able to vary the up-down movement frequency. Figure 7 shows a schematic draw of the model with the electromechanical system inside it:

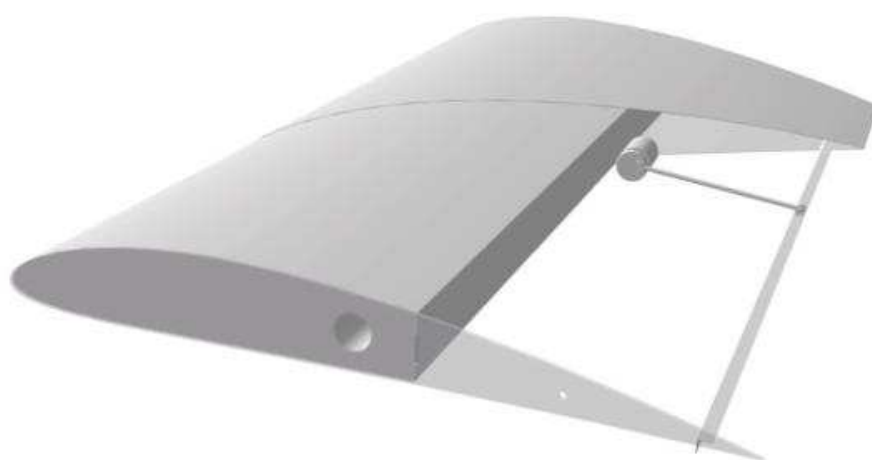


Fig. 7. Schematic draw of the model wing with the electromechanical mechanism

The experiments were carried out in the closed circuit boundary layer wind tunnel of the Boundary Layer & Environmental Fluid Dynamics Laboratory at the Aeronautical Department, Engineering Faculty, National University of La Plata (Argentina). The test section is 1.4m wide, 1m height and 7.5m length and has upstream flow deflectors in order to achieve the desired mean free stream velocity and turbulence intensity.

Figure 8 shows a diagram of the wing model inside the wind tunnel test section. In Figure 9 we show views of the experimental setup, the wing model was mounted between two double lateral plates, which trailing edges were capable to manually adjust along each axis, in order to have a favorable (or almost zero) pressure gradient along the test section, with the thinnest possible boundary layer

Figure 10 shows a schema of the wake measuring positions, along “x” axis and the corresponding vertical points (1H, 2H and 5H), indicating in this Figure only the 0 and -10 points, the separation between vertical adjacent points is 0.25H (2 mm).

A schema of the electromechanical system is shown in Figure 11.

The objective of the experiments carried out at LaCLyFA, were to measure instantaneous velocities in the near wake region, because the near wake structure is directly related with lift production (see also above explanations). Designing with “x” the horizontal coordinate (which is coincident with the model chord line for 0° degree angle of attack) and with “y”

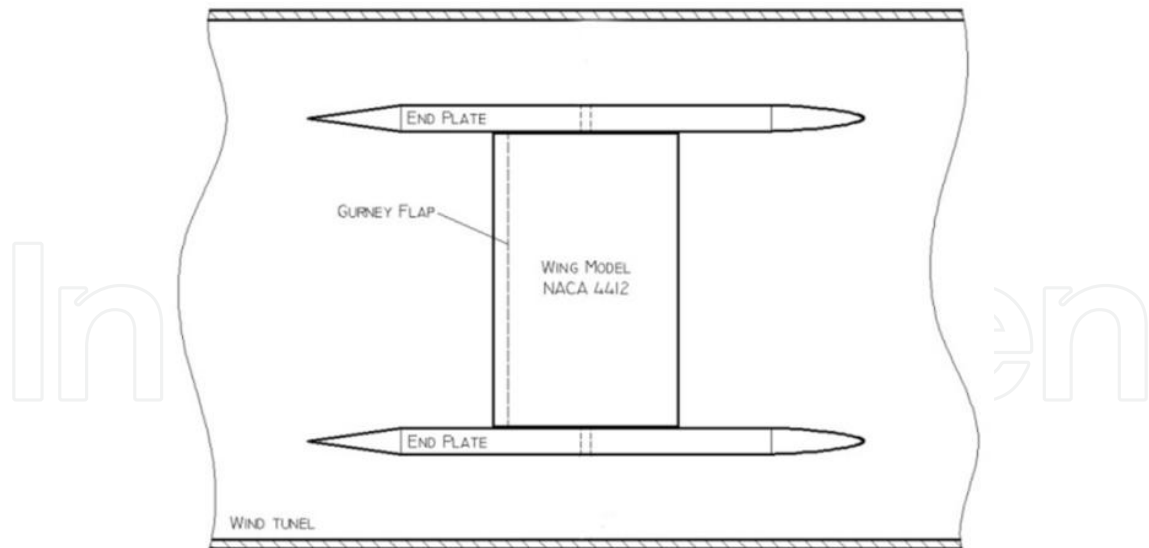


Fig. 8. Diagram of wing model inside the wind tunnel test section

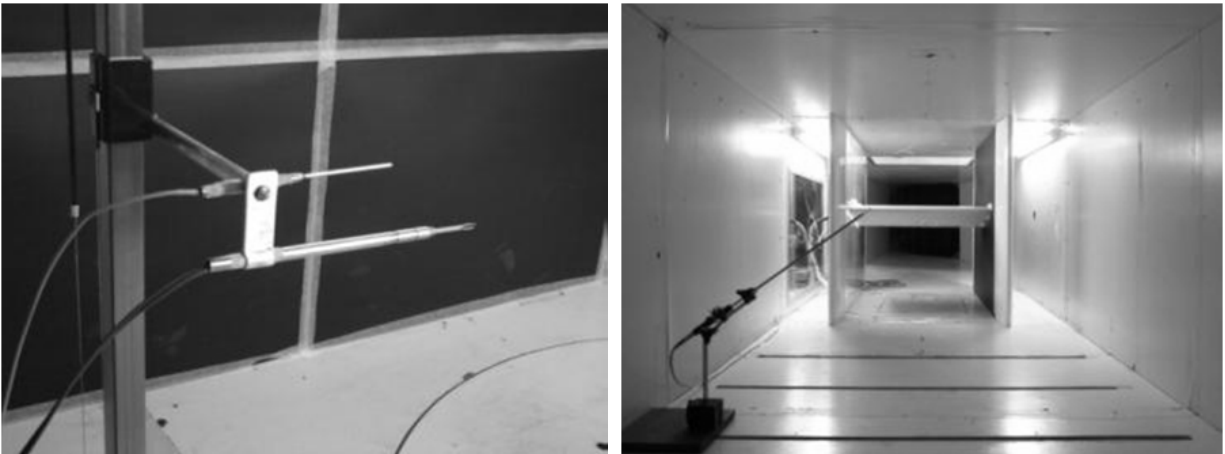


Fig. 9. Experimental setup views.

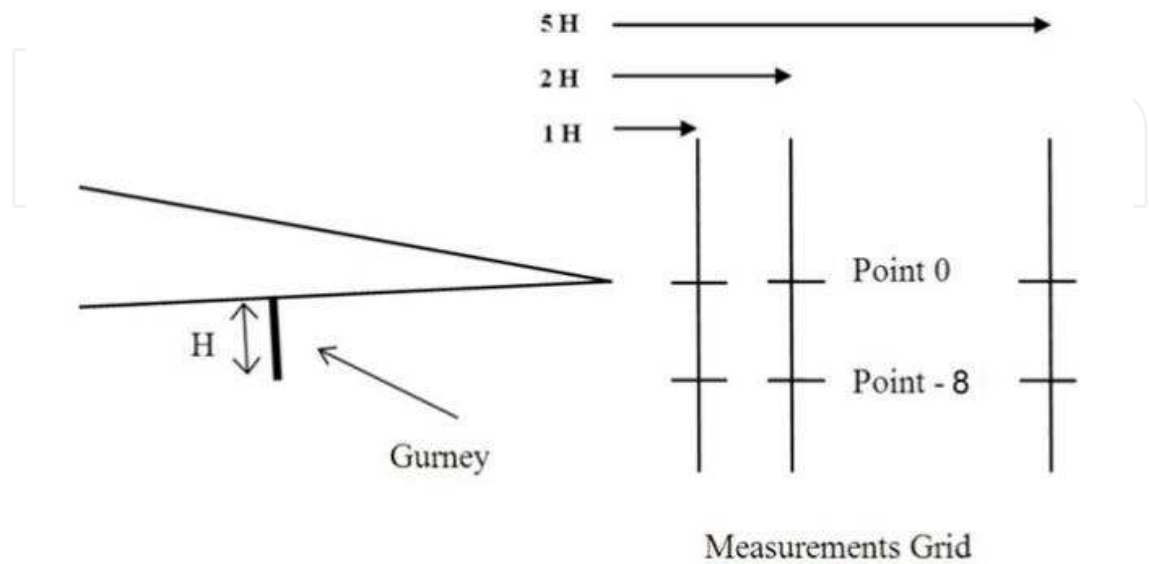


Fig. 10. Measurements Grid

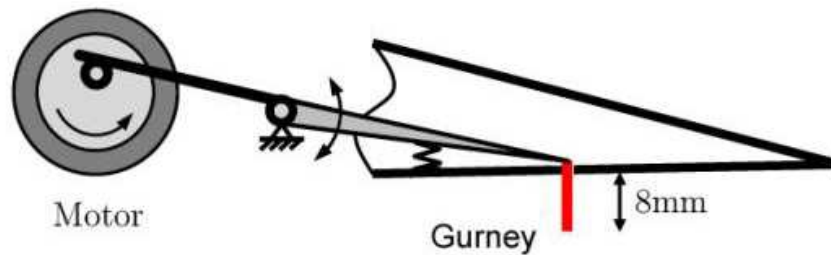


Fig. 11. Mini-flap Gurney type electromechanical movement (schematic).

the vertical coordinate, velocity measurements were performed at $1H$, $2H$ and $5H$ “ x ” positions in the wake, being “ H ” the mini-flap height. For each “ x ” position, vertical measurements were performed from $y = 1H$ to $y = -2H$ with intervals of $0.05H$, being $y = 0$ the trailing edge level.

Velocity data in the near wake, as mentioned above, are very important in order to qualify and quantify the vortex characteristics and structure, together with turbulence intensities, because the possible lift increment is closely related with such near wake structure, that’s, if is strongly asymmetric or not.

Instantaneous velocities were measured with a hot wire constant temperature anemometer Dantec Streamline, using X-probes. The acquisition frequency was 4000 Hz per channel, filtered at 2000 Hz.

The acquired data were very extensive and, for such reason, both research teams (Germany and Argentine teams) for the comparison objectives cited in this work choose results for a determined angle of attack, say 5° degrees.

5. Results analysis (near and medium wake region)

Figure 12 shows the mean velocities U and V , plotted for the five situations—without mini-flap; with fixed deployed mini-flap; oscillating mini-flap for three frequencies, 22Hz (Frequency 1), 38Hz (Frequency 2) and 44Hz (Frequency 3), all for the three “ x ” positions.

Regarding the Figure 12, we could conclude that the U -component has small variations between the different conditions (clean airfoil; fixed flap; etc), being always positive above and below the trailing edge, but with a reduction of its magnitude from the trailing edge level to the end of mini-flap level. The vertical velocities exhibit important differences, above the trailing edge, between the clean airfoil and the fixed mini-flap case. Respect the oscillating mini-flap, there are small differences between the vertical velocities for the three frequencies but, if we look close the vertical velocities at the mini-flap level and lower, their values are greater than the corresponding to clean airfoil or even the fixed mini-flap case. Qualitatively, the situation is similar for all the position. Analyzing the Figure, it’s clear that we have an anticlockwise vortex behind the mini-flap. This is consistent with the results founded by other authors.

Figure 13 shows mean vorticity distribution, along “ x ” coordinate”, evaluated as 2D with the well known expression $\partial V / \partial x - \partial U / \partial y$. In this Figure we show that there is a decrement in the vorticity field downstream the trailing edge, corresponding to the diffusion of the vortex generated by the Gurney flap. Note that the conclusions from the instantaneous

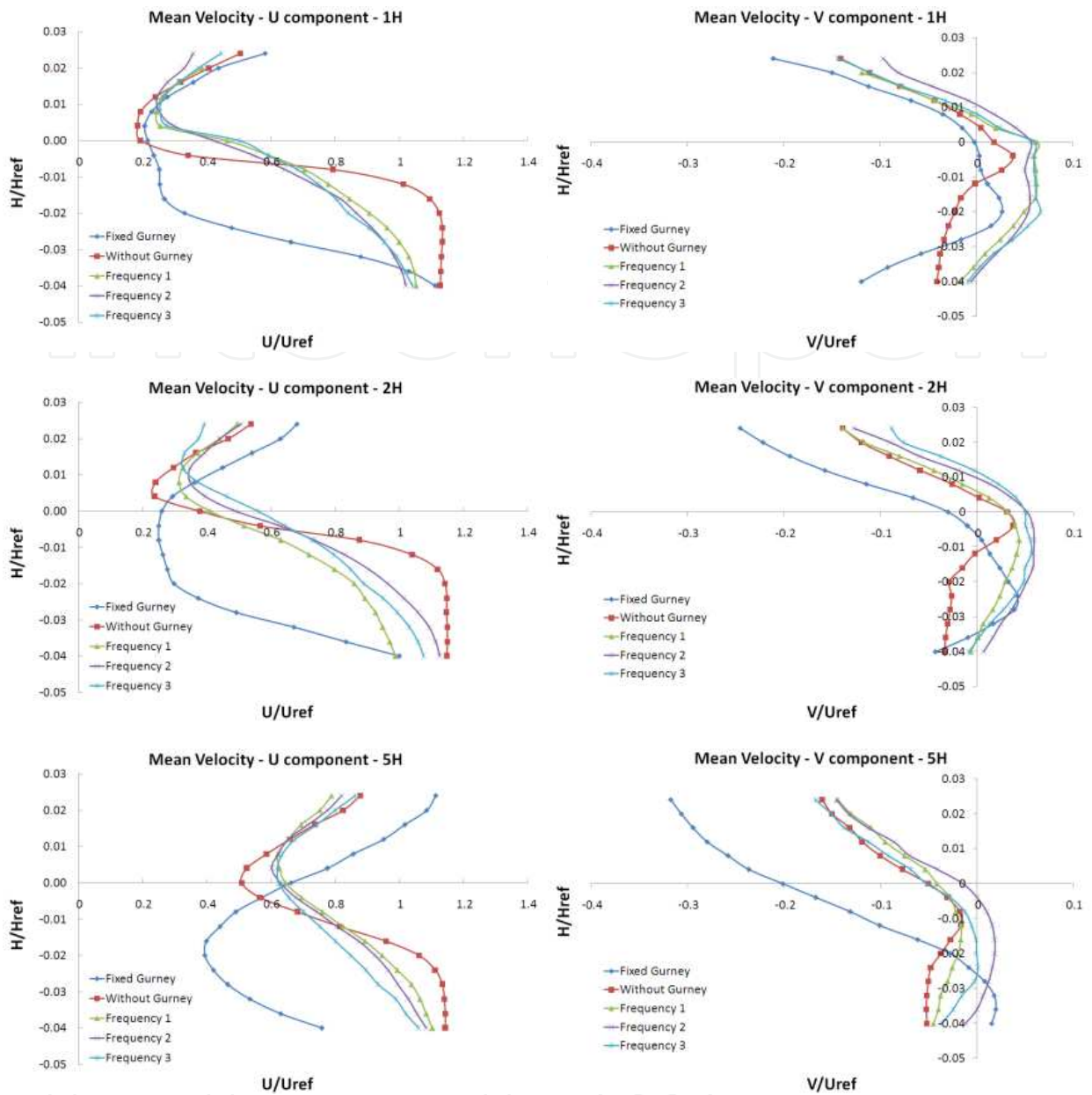


Fig. 12. Mean velocity distributions for the different positions and all the cases.

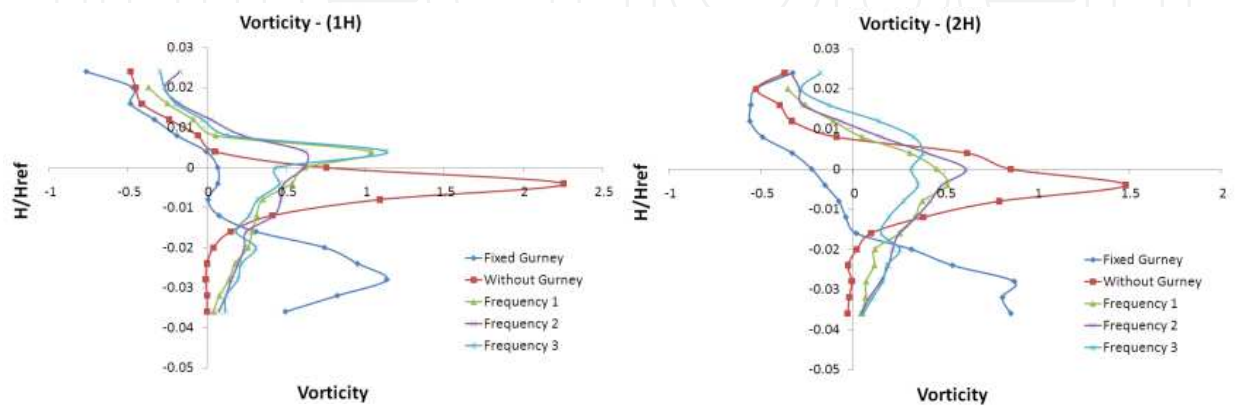


Fig. 13. Mean vorticity distribution along the "x" axis.

vorticity plot of the fluidic Gurney (Figures 2, 3 and 4) hold here as well and are comparable with the mean vorticity calculations showed for the mechanical mini-flap case. The peak positive vorticity in the lower wake is more pronounced than the (negative) vorticity in the upper wake. This is true for all cases.

Figure 14 corresponds to turbulence intensities for the three “x” positions. Again the flow turbulent intensities diminish as we move downstream the trailing edge, showing to us that the vortex generated by the Gurney seems to disappear after 5H position.

Regarding Figure 15, almost all positions didn't revealed the spectra peak from the Gurney vortex downstream, except for the movable one that show us a series of peaks referring the activity of the flap. Also, the peaks found in some of them are related to the frequencies of

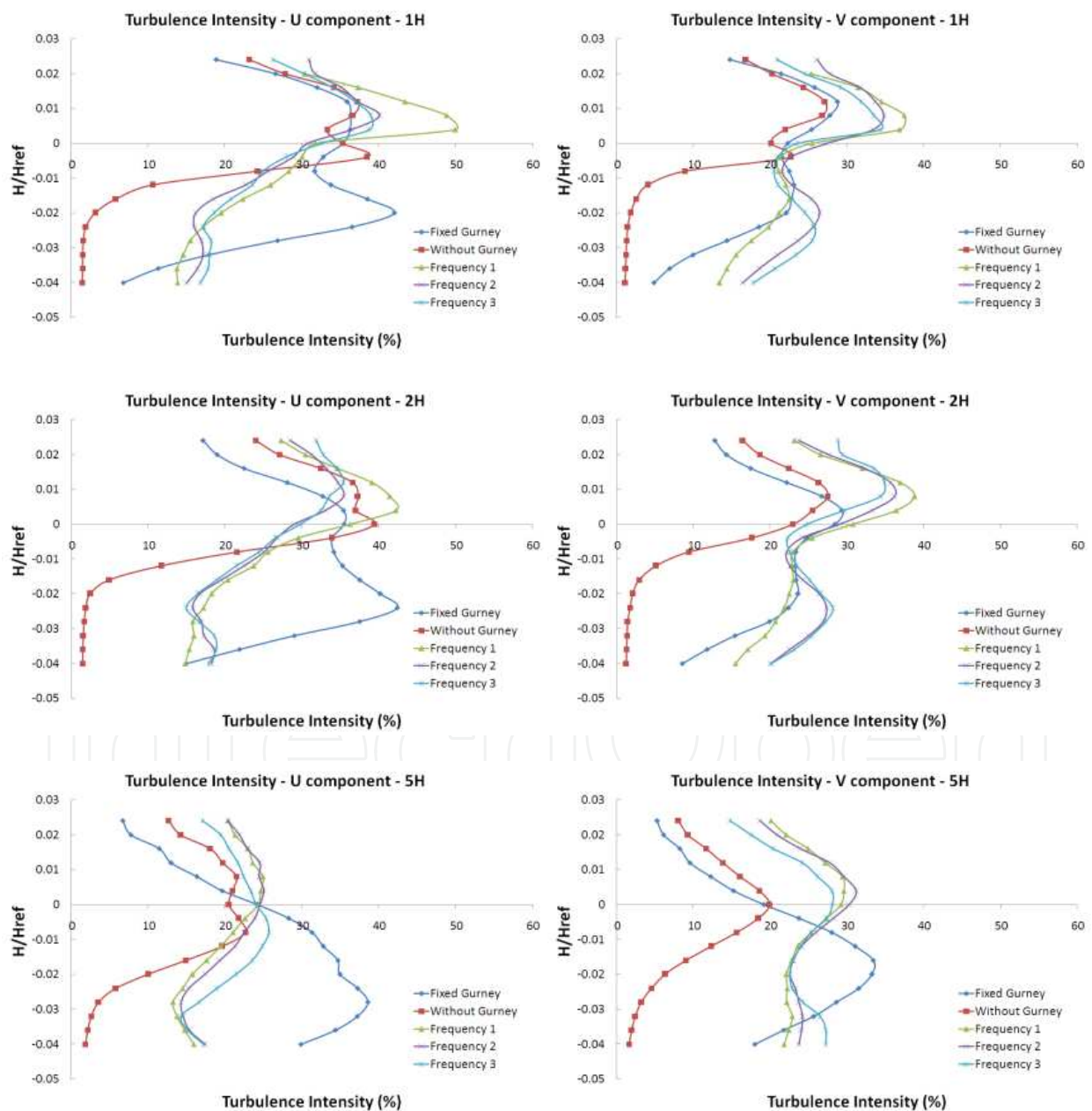


Fig. 14. Turbulence intensity distribution for the U and V component in all cases

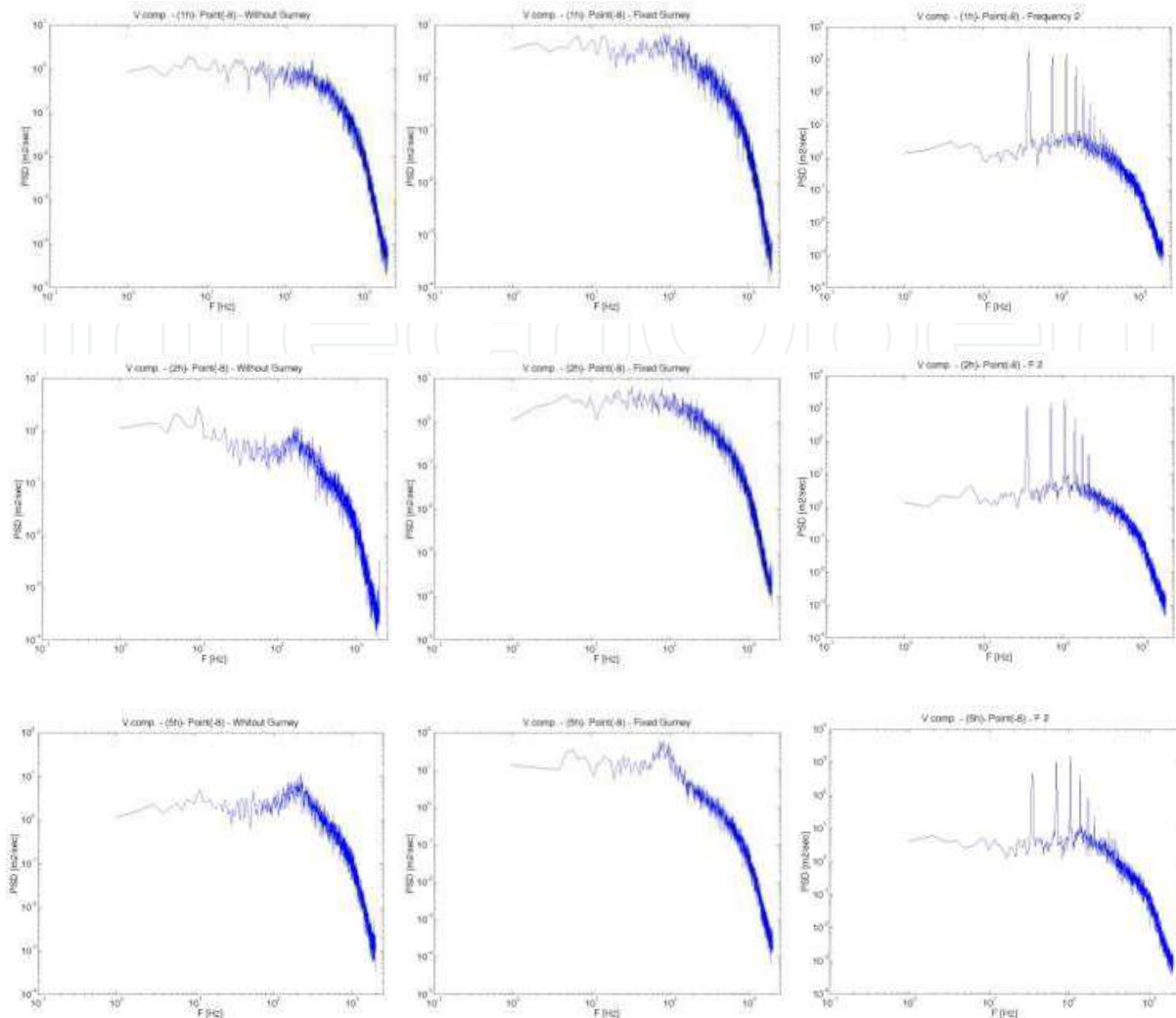


Fig. 15. Power Density Spectra at point -8, with and without Gurney Flap, and the movable one at frequency 2. In the location at 1, 2 and 5 H positions, downstream the trailing edge airfoil at 5° angle of attack.

the vortex release by the airfoil and not with those generated by the fixed Gurney (200 Hz approximately). This means that the Gurney downstream is outside the measured grid, except for the case of 5H at point -8 for the fixed Gurney, in which the 96 Hz peak show to us the presence of the Gurney vortex downstream. From this behavior we can conclude, for this angle of attack, that the vortex generated by the Gurney flap it is moving downstream and will be catch a long distances from the trailing edge before it becomes diffuse at the far wake.

Figures 16, 17 and 18 corresponds to the autocorrelation coefficients, at 1H, for horizontal and vertical instantaneous velocities, for the case with fixed miniflap and the oscillatory one for Frequencies 1 and 3, respectively. Figures 19 to 21, corresponds to the autocorrelations coefficients, at 2H, as previous Figures but for Frequencies 1 and 2. Finally, Figures 22 to 23 referred also to the autocorrelation coefficients, as Figures 16 to 18, but for 5H.

Table 1 also shows temporal and spatial scales for the horizontal and vertical components of the mean velocities in the near wake, for the five situations: without miniflap; fixed miniflap and oscillatory one (three excitation frequencies).

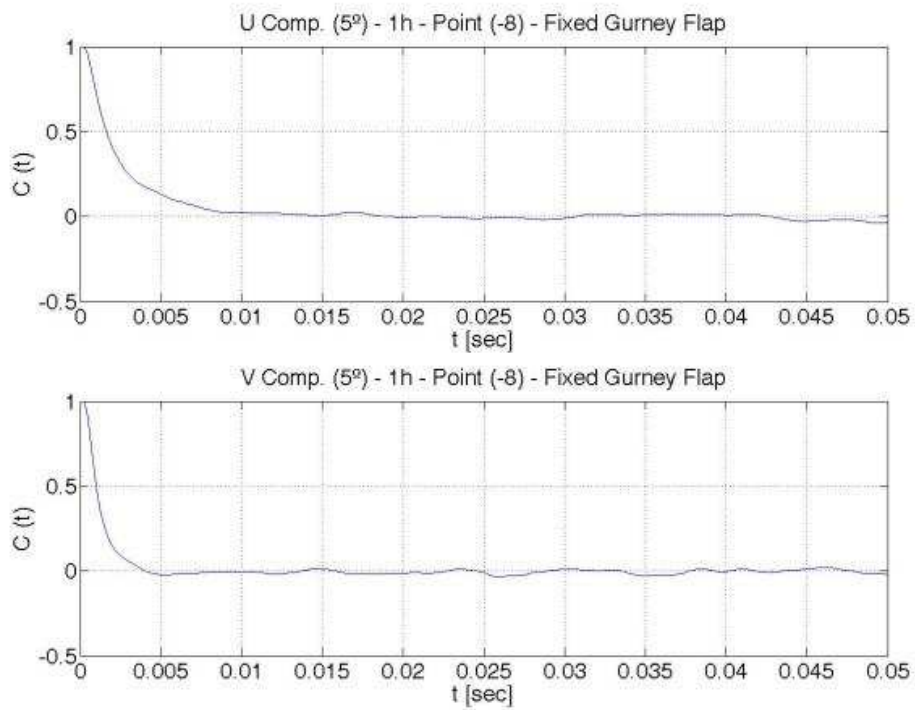


Fig. 16. Autocorrelation coefficients for 1H at fixed Gurney.

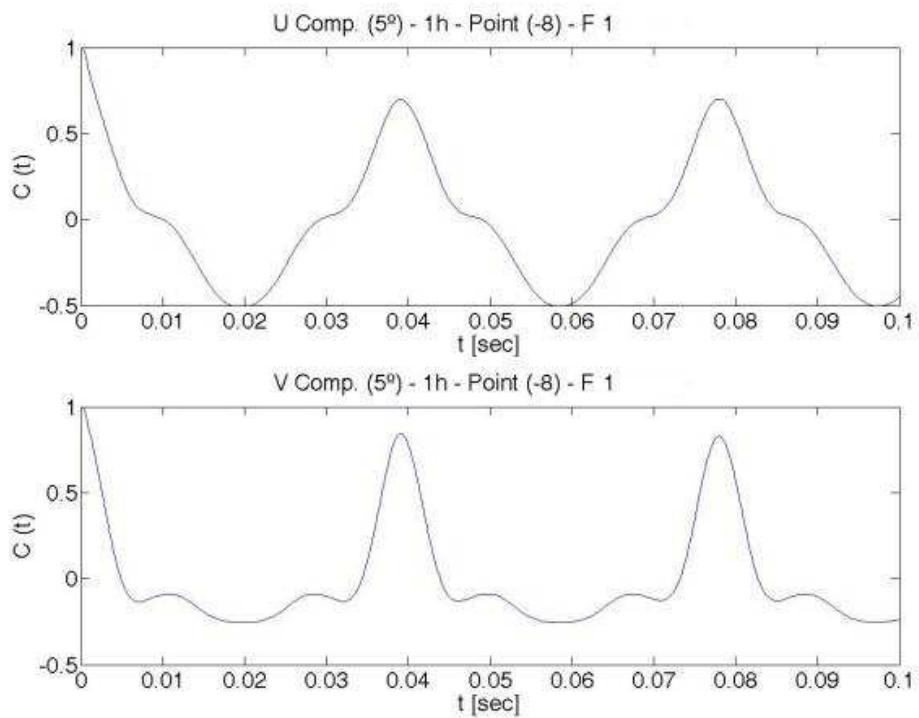


Fig. 17. Autocorrelation coefficients for 1H at Frequency 1.

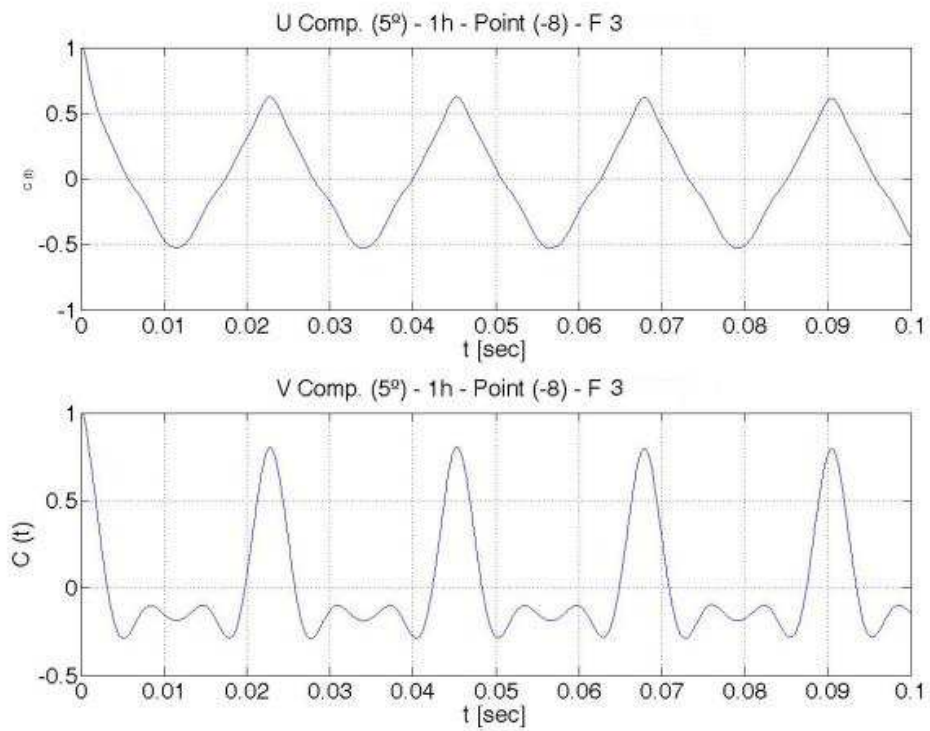


Fig. 18. Autocorrelation coefficients for 1H at Frequency 3.

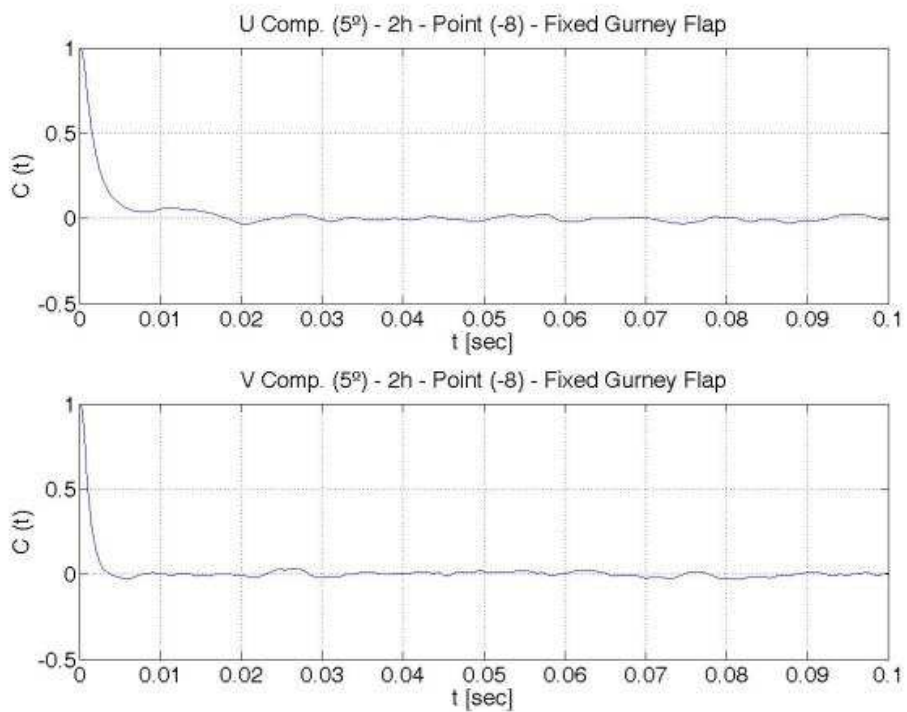


Fig. 19. Autocorrelation coefficients for 2H at fixed Gurney.

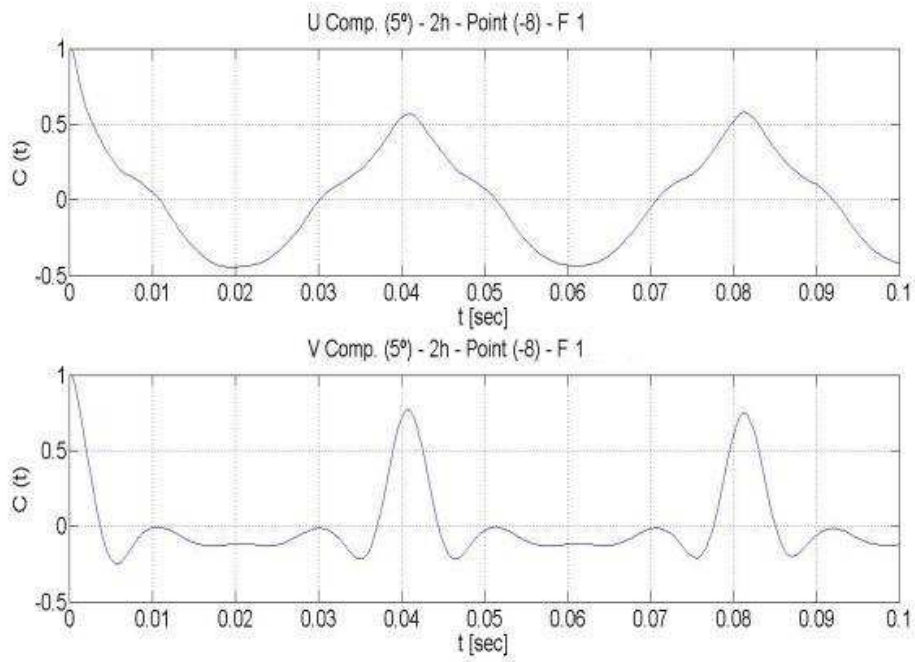


Fig. 20. Autocorrelation coefficients for 2H at Frequency 1.

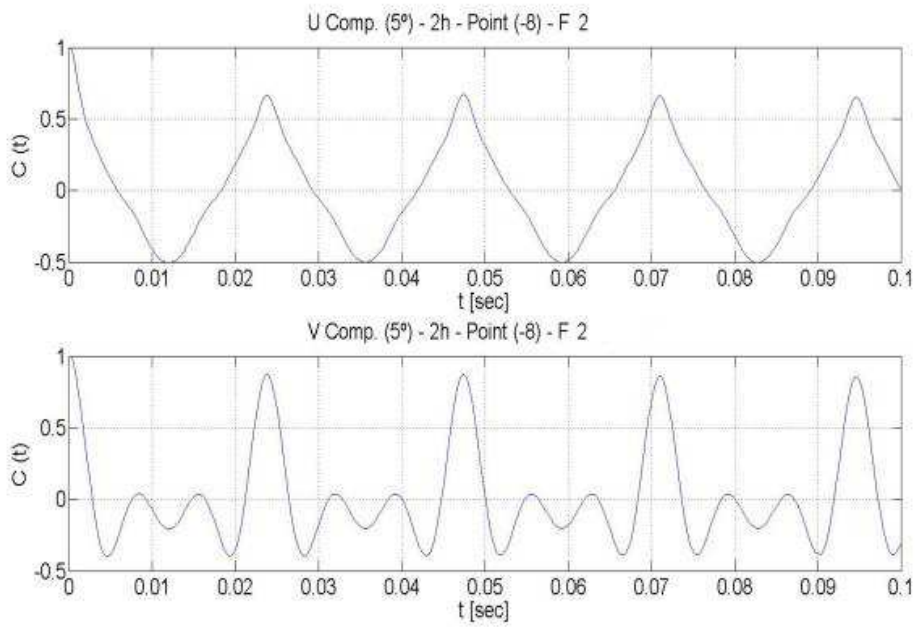


Fig. 21. Autocorrelation coefficients for 2H at Frequency 2.

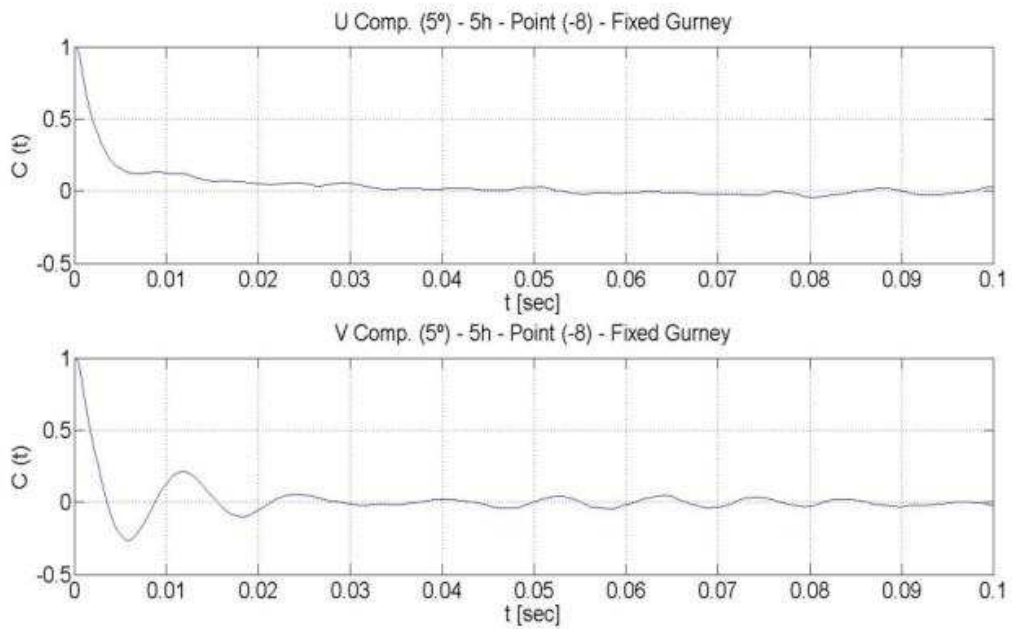


Fig. 22. Autocorrelation coefficients for 5H at fixed Gurney.

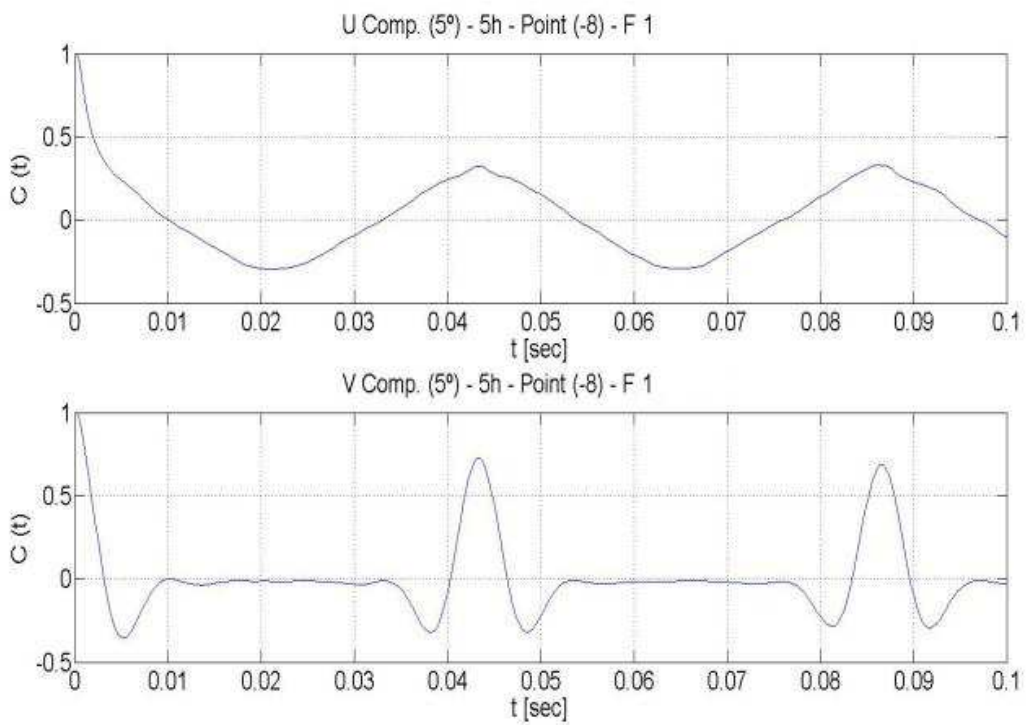


Fig. 23. Autocorrelation coefficients for 5H at Frequency 1.

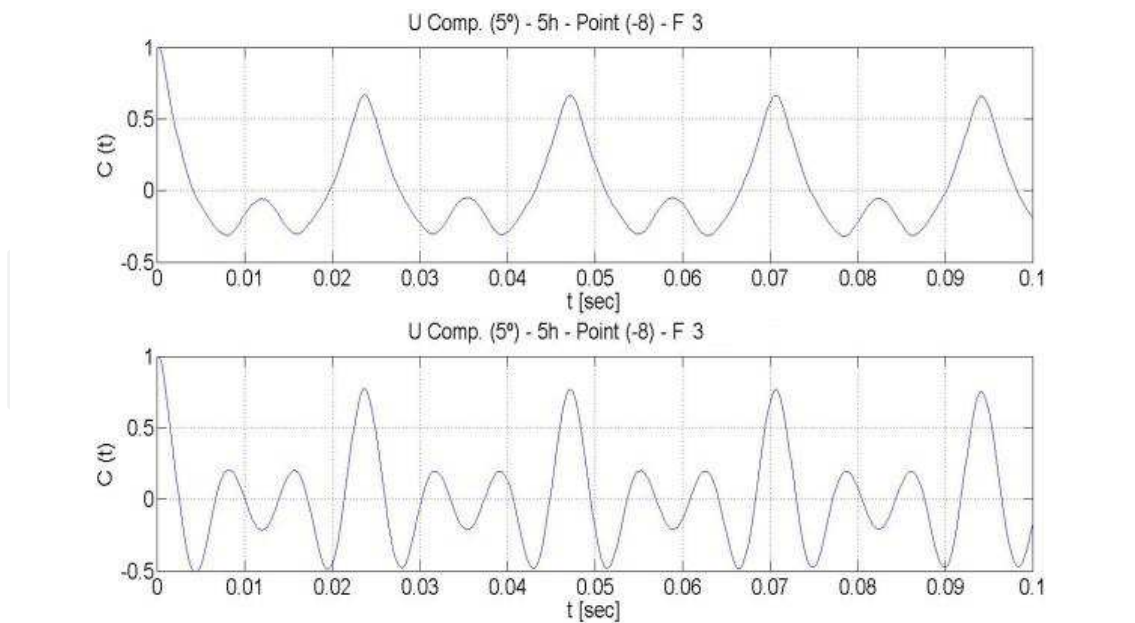


Fig. 24. Autocorrelation coefficients for 5H at Frequency 3.

1H	Device	tu [sec]	tv [sec]	U [m/sec]	V [m/sec]	Eu [m]	Ev [m]
	Without Gurney	0.01350	0.03950	10.955	0.156	0.14789	0.00616
	Fixed Gurney	0.01875	0.00400	2.688	0.236	0.05040	0.00094
	Frequency 1	0.00975	0.00500	8.454	0.615	0.08243	0.00308
	Frequency 2	0.00675	0.00325	8.178	0.557	0.05520	0.00181
	Frequency 3	0.00575	0.00325	8.025	0.623	0.04614	0.00202

2H	Device	tu [sec]	tv [sec]	U [m/sec]	V [m/sec]	Eu [m]	Ev [m]
	Without Gurney	0.01275	0.00200	11.210	0.152	0.14293	0.00030
	Fixed Gurney	0.01800	0.00400	2.780	0.236	0.05004	0.00094
	Frequency 1	0.01075	0.00375	7.986	0.363	0.08585	0.00136
	Frequency 2	0.00775	0.00300	9.066	0.580	0.07026	0.00174
	Frequency 3	0.00575	0.00275	8.489	0.500	0.04881	0.00138

5H	Device	tu [sec]	tv [sec]	U [m/sec]	V [m/sec]	Eu [m]	Ev [m]
	Without Gurney	0.01475	0.00150	9.590	0.271	0.14145	0.00041
	Fixed Gurney	0.05275	0.00350	3.987	0.615	0.21031	0.00215
	Frequency 1	0.01000	0.00325	8.940	0.170	0.08940	0.00055
	Frequency 2	0.00727	0.00300	8.742	0.186	0.06355	0.00056
	Frequency 3	0.00425	0.00250	8.017	0.010	0.03407	0.00003

Table 1. Temporal (tu and tv) and Spatial (Eu and Ev) scales for u and v velocities components.

As a first plain sight we could establish that:

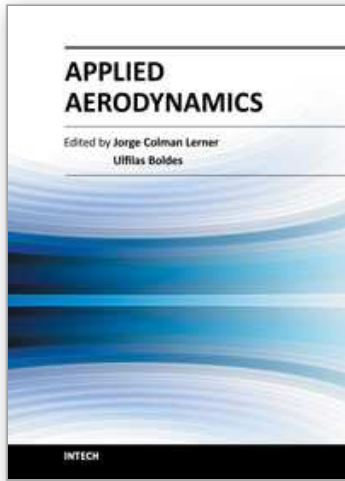
- a. Regarding turbulence intensity and spatial scales also, along “x” coordinate, it seems to slow both as miniflap frequency grow. This behavior was observed, also, for the wing model with the mechanical miniflap, at an angle of attack of 0°. Due space reasons of this article, we don’t show also the results for such angle of attack.
- b. Mean vertical velocity V is greater for the moving flap than for the fixed one, all in the near wake region. This effect becomes lower as we go far away the near wake.

- c. Mean vorticity, always in the near wake region, seems to become slow with the fixed mini-flap in comparison with the clean airfoil and, as oscillating frequency increase, such mean vorticity diminishing effect becomes more important than with the fixed mini-flap. The mean vorticity behavior is similar to the results obtained by Wassen et al [14], at the same points measured by us in the present work.
- d. The above cited behavior of the mean vorticity, at the near wake, has a good match with the instantaneous vorticity results provided by fluidic miniflap experiments. Due the fact that the vorticity calculations for the mechanical miniflap are done with the mean velocities, and for the fluidic miniflap were done with the instantaneous velocities, the mentioned similar behavior of both experiments is qualitative but, in that sense, the agreement is good.
- e. As the angle of attack grows, vertical mean velocity becomes more important than horizontal one.

The above summarized analysis encourage us to go deep, in the future, into the study of the effects of fluidic and mechanical miniflaps upon lift behavior and, hence, upon aerodynamic efficiency of airfoils with such active flow control mechanism.

6. References

- [1] C. Hah et al, Measurement and prediction of mean velocity and turbulence structure in the near wake of an airfoil, *Journal of Fluid Mechanics*. Vol.115, 1982 pp. 251-282.
- [2] R.H. Liebeck, Design of subsonic airfoils for high lift, *Journal of Aircraft* Vol. 15, No. 9, 1978, pp 547-561.
- [3] D.H. Neuhart et al, A water tunnel study of Gurney flaps, *NASA TM-4071*, 1988.
- [4] A.W. Bloy, Aerodynamic Characteristics of an aerofoil with Small Trailing Edge Flaps, *Wind Engineering*, Vol. 19, No.3, 1995, pp 167-172.
- [5] B.L. Storms, Lift Enhancement of an Airfoil Using a Gurney Flap and Vortex Generators, *Journal of Aircraft* Vol. 31, No. 3, 1994, pp 542-547.
- [6] P. Giguère, J. Lemay, G. Dumas, Gurney Flap Effects and Scaling for Low-Speed Airfoils, *AIAA Paper 95-1881*, 13th AIAA Applied Aerodynamics Conference San Diego, 1995.
- [7] D.R.M. Jeffery, D.W. Hurst, Aerodynamics of the Gurney Flap, *AIAA Applied Aerodynamic Conference*, AIAA 96-2418-CP, 1996.
- [8] D. Jeffrey et al, Aerodynamics of Gurney Flaps on a Single-Element High-Lift Wing, *Journal of Aircraft*, Vol. 37, 2000, pp. 295-301.
- [9] F. Bacchi, J. Marañón Di Leo, J.S. Delnero, J. Colman, M. Martinez, M. Camocardi, U. Boldes, Determinación experimental del efecto de mini flaps Gurney sobre un perfil HQ-17, *Fluidos-2006 IX Reunión Sobre Recientes Avances En Física de Fluidos y sus Aplicaciones*, Mendoza, Argentina, 2006.
- [10] C.P. Van Dam et al, Gurney Flap Experiments on Airfoil and Wings, *Journal of Aircraft* (0021-8669), Vol.36, No.2, 1999, pp. 484-486.
- [11] D.W. Bechert, R. Meyer, W. Hage, Drag Reduction of Airfoils with Miniflaps. Can We Learn From Dragonflies?, *AIAA-2000-2315*, Denver, CO, 2000.
- [12] M. Schatz, B. Guenther, F. Thiele, Computational Modeling of the Unsteady Wake behind Gurney-Flaps, *2nd AIAA Flow Control Conference*, AIAA-2417, Portland, Oregon, USA, 2004.
- [13] Garner, H.C., Rogers, E.W.E., Acum, W.E.A., Maskell, E.C., Subsonic Wind Tunnel Wall Corrections, *AGARDograph* 109, 1966
- [14] E. Wassen, B. Gunther, F. Thiele, J. Marañón Di Leo, J.S. Delnero, J. Colman, U. Boldes. A Combined Numerical and Experimental Study of Mini-Flaps at Varying Positions on an Airfoils. 45th AIAA Aerospace Sciences Meeting and Exhibit, Reno, 8-11 January 2007. Actas del Congreso.



Applied Aerodynamics

Edited by Dr. Jorge Colman Lerner

ISBN 978-953-51-0611-1

Hard cover, 192 pages

Publisher InTech

Published online 11, May, 2012

Published in print edition May, 2012

Aerodynamics, from a modern point of view, is a branch of physics that study physical laws and their applications, regarding the displacement of a body into a fluid, such concept could be applied to any body moving in a fluid at rest or any fluid moving around a body at rest. This Book covers a small part of the numerous cases of stationary and non stationary aerodynamics; wave generation and propagation; wind energy; flow control techniques and, also, sports aerodynamics. It's not an undergraduate text but is thought to be useful for those teachers and/or researchers which work in the several branches of applied aerodynamics and/or applied fluid dynamics, from experiments procedures to computational methods.

How to reference

In order to correctly reference this scholarly work, feel free to copy and paste the following:

M. Casper, P. Scholz, J. Colman, J. Marañón Di Leo, S. Delnero and M. Camocardi (2012). Comparison of Aerodynamic Effects Promoted by Mechanical and Fluidic Miniflaps on an Airfoil NACA 4412, *Applied Aerodynamics*, Dr. Jorge Colman Lerner (Ed.), ISBN: 978-953-51-0611-1, InTech, Available from: <http://www.intechopen.com/books/applied-aerodynamics/comparison-of-aerodynamic-effects-promoted-by-mechanical-and-fluidic-miniflaps-on-an-airfoil-naca-44>

INTECH
open science | open minds

InTech Europe

University Campus STeP Ri
Slavka Krautzeka 83/A
51000 Rijeka, Croatia
Phone: +385 (51) 770 447
Fax: +385 (51) 686 166
www.intechopen.com

InTech China

Unit 405, Office Block, Hotel Equatorial Shanghai
No.65, Yan An Road (West), Shanghai, 200040, China
中国上海市延安西路65号上海国际贵都大饭店办公楼405单元
Phone: +86-21-62489820
Fax: +86-21-62489821

© 2012 The Author(s). Licensee IntechOpen. This is an open access article distributed under the terms of the [Creative Commons Attribution 3.0 License](#), which permits unrestricted use, distribution, and reproduction in any medium, provided the original work is properly cited.

IntechOpen

IntechOpen